Modeling and design of Galfenol unimorph energy harvester

Deng, Zhangxian, Dapino, Marcelo

Zhangxian Deng, Marcelo J. Dapino, "Modeling and design of Galfenol unimorph energy harvester," Proc. SPIE 9057, Active and Passive Smart Structures and Integrated Systems 2014, 90572A (1 April 2014); doi: 10.1117/12.2047113

SPIE.

Event: SPIE Smart Structures and Materials + Nondestructive Evaluation and Health Monitoring, 2014, San Diego, California, United States

Modeling and design of Galfenol unimorph energy harvester

Zhangxian Deng, Marcelo J. Dapino

Smart Vehicle Concepts Center, Department of Mechanical and Aerospace Engineering,
The Ohio State University, Columbus, OH, USA, 43210

ABSTRACT

Magnetostrictive iron-gallium alloys, known as Galfenol, are a recent class of smart materials with potential in energy harvesting applications. Unimorph energy harvesters consisting of a Galfenol beam bonded to a passive substrate are simple and effective, but advanced models are lacking for these smart devices. This study presents a finite element model for Galfenol unimorph harvester systems. Experiments considering various design parameters such as pick up coil size, load resistance, beam thickness ratio, and bias magnetic field strength are conducted to guide and validate the modeling effort. If the free length of the Galfenol unimorph beam is considered as the effective length, the maximum average power density, peak power density, and open-circuit voltage amplitude achieved in experiments are 13.97 mW/cm^3, 35.51 mW/cm^3, and 0.66 V, respectively. By only considering the length of Galfenol surrounded by the pickup coil, the maximum average power density and peak power density are 23.66 mW/cm^3 and 60.14 mW/cm^3, respectively.

Keywords: Galfenol, Energy Harvester, Unimorph, COMSOL Multiphysics

1. INTRODUCTION

Iron-gallium Galfenol alloys are a recent class of giant magnetostrictive materials that exhibit moderate magnetostriction (around 400 ppm) and magnetization (around 1200 kA/m).[1] Unlike brittle Terfenol-D and piezoelectric materials, Galfenol has a high mechanical tensile strength (500 MPa)[2] while being able to support shear and shock loads. As an iron alloy, Galfenol can be machined, welded and formed. Without undergoing permanent depolarization, Galfenol also maintains significant magnetomechanical coupling over a broad temperature range.[3,4] Hence, Galfenol has potential in actuator, sensor and energy harvester designs.

The reduction in size and power consumption of embedded and wireless sensors has motivated the development of built-in structural energy sources. Vibration-based energy harvesters scavenge energy from vibrating structures. They reduce or eliminate the need for batteries and improve overall energy efficiency. Vibration-based energy harvesters using passive materials have been successfully implemented. Meninger et al.[5] developed an electrostatic harvester which is a variable capacitor to convert mechanical kinetic energy to electrical energy. Glynne-Jones et al.[6] designed and optimized an electromagnetic harvester based on moving magnets inside a static coil.

Compared with traditional passive energy harvesters, smart materials including piezoelectric and magnetostrictive materials help to enhance the energy conversion efficiency and reduce system mass and bulk. Beeby et al.[7] reviewed several existing piezoelectric generators for microsystem applications and showed that

Further author information: (Send correspondence to M.J.D)
Z.D.: E-mail: deng.92@osu.edu, Telephone: 1-614-886-4687
M.J.D.: E-mail: dapino.1@osu.edu, Telephone: 1-614-688-3689

Active and Passive Smart Structures and Integrated Systems 2014, edited by Wei-Hsin Liao, Proc. of SPIE Vol. 9057, 90572A · © 2014 SPIE
CCC code: 0277-786X/14/$18 · doi: 10.1117/12.2047113

the maximum power density of these devices is about 0.37 mW/cm^3.[8] Research on piezomagnetoelastic energy harvesters yielded an output power density of 13 mW/cm^3.[9] Wang and Yuan[10] implemented a Metglas beam as a vibratory energy harvester and obtained an output power density of 0.9 mW/cm^3. Berbyuk[11] presented a Galfenol harvester which converts axial vibration energy to electrical energy achieving a power density of 338 mW/cm^3. Yoo and Flatau[12,13] developed a unimorph energy harvester in bending mode and proved its feasibility over a range of temperatures. Ueno and Yamada[14] proposed a bimorph Galfenol harvester and observed a maximum peak power density of 200 mW/cm^3. The literature therefore suggests that energy harvesters based on magnetostrictive materials achieve power densities similar to piezoelectric harvesters. However, harvesters based on magnetostrictive materials suffer no depolarization issues and have a favorably low output impedance.

One limitation of current magnetostrictive harvester designs is the lack of accurate and computationally efficient device models. Yoo and Flatau[12] simplified the unimorph device into a spring-damper-mass model but the model significantly over predicts the output voltage from the pickup coil. Wang and Yuan[10] developed a magnetostrictive beam model based on continuous vibration theory, but they utilized a linearized material model that also over predicts the output. FEA models proposed by Chakrabarti et al.[15] and modified by Deng et al.[16] accurately describe the dynamic nonlinear Galfenol response but they are not sufficiently efficient to be implemented in model-guided design. Rezaeealam et al.[17] implemented Armstrong's model to generate interpolation functions and presented a static 3D FEA model built in COMSOL Multiphysics for Galfenol-based bimorph harvesters. Accurate flux density calculations were presented, but no parametric studies were proposed.

In this study, a simplified 2D FEA model is first derived for efficient parametric studies. Five different unimorph harvesters are tested to validate the proposed model. Load match testing is conducted to analyze the power output of the unimorph harvester. Finally, a parametric study is presented in which the sensitivity of device performance to thickness ratio, coil size, and bias magnetic field strength is analyzed.

2. THEORY

2.1 Discrete Energy Average Model

Constitutive Galfenol models have been successfully developed. Armstrong[18] first presented an energy-based model for Galfenol and Restorff et al.[2] simplified this model by reducing the number of material easy directions to 98. Evans and Dapino[19] further reduced the number of easy directions to six and constructed a discrete energy average (EA) model for cubic symmetric Galfenol based on local energies calculated in the vicinity of the easy directions. The local Gibbs energy in the EA model is defined as

$$G^k = \frac{1}{2}K^k|\mathbf{m}^k - \mathbf{c}^k|^2 - \mathbf{S}_m^k \cdot \mathbf{T} - \mu_0 M_s \mathbf{m}^k \cdot \mathbf{H}, \tag{1}$$

where k denotes the number of easy directions, K^k is the anisotropy constant, $\mathbf{m}^k$ is the moment orientation, $\mathbf{S}_m^k$ is the magnetostriction, $\mathbf{T}$ is the stress tensor, and $\mathbf{H}$ is the magnetic field vector.

The orientations of Galfenol moments are calculated through minimization of (1). Assuming $||\mathbf{m}^k|| \approx \mathbf{m}^k \cdot \mathbf{c} = 1$, the analytical solution for moment orientations $\mathbf{m}^k$ can be written as

$$\mathbf{m}^k = (\mathbf{K}^k)^{-1}\left[\mathbf{B}^k + \frac{1 - \mathbf{c}^k \cdot (\mathbf{K}^k)^{-1}\mathbf{B}^k}{\mathbf{c} \cdot (\mathbf{K}^k)^{-1}\mathbf{c}^k}\mathbf{c}^k\right], \tag{2}$$

where λ_{100} is the maximum magnetostriction, λ_{111} is the maximum shear magnetostriction,

$$\mathbf{K}^k = \begin{bmatrix} K^k - 3\lambda_{100}T_1 & -3\lambda_{111}T_4 & -3\lambda_{111}T_6 \\ -3\lambda_{111}T_4 & K^k - 3\lambda_{100}T_2 & -3\lambda_{111}T_5 \\ -3\lambda_{111}T_6 & -3\lambda_{111}T_5 & K^k - 3\lambda_{100}T_3 \end{bmatrix}, \tag{3}$$

and

$$\mathbf{B}^k = \begin{bmatrix} c_1^k K^k + \mu_0 M_s H_1 & c_2^k K^k + \mu_0 M_s H_2 & c_3^k K^k + \mu_0 M_s H_3 \end{bmatrix}^T. \tag{4}$$

The bulk magnetization $\mathbf{M}$ and magnetostriction $\mathbf{S}_m$ are the weighted sum of the magnetization $M_s\mathbf{m}^k$ and magnetostriction $\mathbf{S}_m^k$ due to each orientation,

$$\mathbf{M} = M_s \sum_{k=1}^{6} \xi^k \mathbf{m}^k, \quad \mathbf{S}_m = \sum_{k=1}^{6} \xi^k \mathbf{S}_m^k, \tag{5}$$

where ξ^k is the weight or volume fraction of the k^{th} orientation.
The magnetostriction of a cubic symmetric particle can be written as[20]

$$\mathbf{S}_m^k = \begin{bmatrix} (3/2)\lambda_{100}(m_1^k)^2 \\ (3/2)\lambda_{100}(m_2^k)^2 \\ (3/2)\lambda_{100}(m_3^k)^2 \\ 3\lambda_{111}m_1^k m_2^k \\ 3\lambda_{111}m_3^k m_2^k \\ 3\lambda_{111}m_1^k m_3^k \end{bmatrix}, \tag{6}$$

where $\mathbf{m}^k = [m_1^k, m_2^k, m_3^k]$. The volume fraction ξ^k of each orientation is calculated through a Boltzmann-type, energy weighting expression:

$$\xi^k = \frac{e^{-G^k/\Omega}}{\sum_{k=1}^{6} e^{-G^k/\Omega}}, \tag{7}$$

where Ω is the Armstrong smoothing factor.[18]

This study implements the EA model to generate interpolation functions for COMSOL Multiphysics v4.3b. The Galfenol material used in this study is rolled and heat treated as provided by Etrema Products, Inc. (Table 1). These material property values have proven accurate in previous research.[15,21,22]

Table 1. Galfenol material properties used in this study.

K_{100} (kJ/m^3)	λ_{100} (ppm)	λ_{111} (ppm)	Ω (J/m^3)	E_s (GPa)	$\mu_0 M_s$ (T)
30	2/3*280	-20/3	1200	60	1.6

2.2 2D COMSOL Multiphysics model

The 3D fully nonlinear anhysteretic FEA model[15,16] for the unimorph harvester shown in Figure 1 is first implemented to investigate whether or not a simplified 2D FE model is sufficiently accurate. The thickness ratio of the unimorph beam, defined as the thickness of the substrate layer over the thickness of the Galfenol layer, is set to 1. The remanent flux density of the tip magnet is 1.8 T. Figure 2 and Figure 3 are a sliced-view of the quasi-static flux density and magnetostriction through the center of the Galfenol layer in the x-y plane. Compared with the flux density B_x along the length (x-axis) (Figure 2(a)), the flux density B_y along

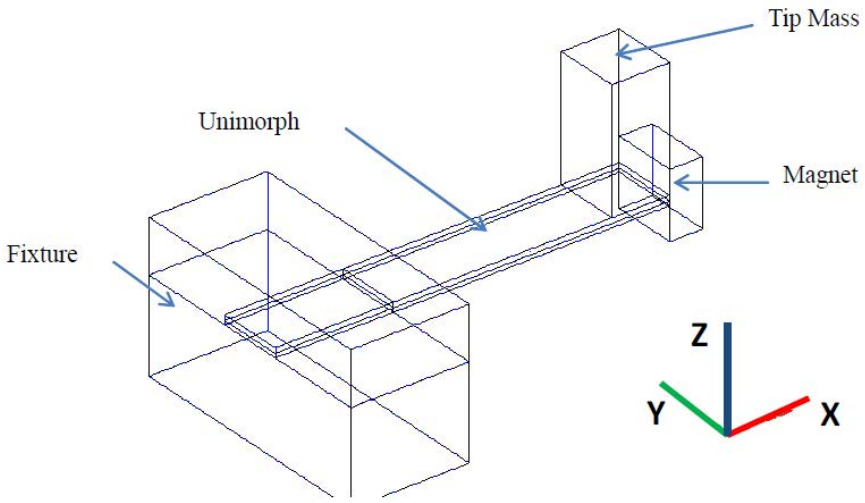

Figure 1. Geometry of 3D unimorph beam harvester in COMSOL Multiphysics.

the width (y-axis) (Figure 2(b)) is negligible except near the magnet's end. Figure 2(a) also demonstrates that the variation of B_x along the width is insignificant excluding the region close to the edges. The same characteristics are observed in the magnetostriction calculations. Figure 3 shows that the magnetostriction λ_{xx} along the x-axis is homogeneous along the y-axis and a 2D model in the x-z plane is a reasonable simplification for both magnetic and mechanical domains. A key advantage of the 2D model is that it greatly reduces simulation time.

Because the damping ratio of the unimorph beam is small, most of the simulation time would be spent on computing the transient state if the dynamic base excitation was directly applied. This study further simplifies the simulation by dividing it into two steps. In the first step, the Galfenol layer is considered as a passive material with constant modulus. According to experimental results on unimorph resonance frequencies, the equivalent Young's modulus of Galfenol is about 54 GPa. The COMSOL Multiphysics eigenfrequency solver is implemented to obtain both natural frequencies and tip displacement amplitudes. In the second step, the calculated tip displacement is assumed to be a sinusoidal function and applied as a boundary condition to the 2D Galfenol model. The 2D FEA model is computed in quasi-static mode to evaluate the average flux density through the cross-section of the pickup coil. The output voltage V is calculated through Faraday's law

$$V = -NA\frac{dB}{dt}, \tag{8}$$

where NA is the coil constant. The value of NA is set at 150 cm^2 in this study. Through the above simplifications, magnetic field dynamics and Galfenol hysteresis are ignored. The unimorph beam model reaches steady state after only 2 cycles.

The nonlinear field-flux density (H-B) relationship of the Galfenol layer is described using an interpolation function H(B_x, T_{xx}) in COMSOL Multiphysics v4.3b, where B_x is the flux density along the length and T_{xx} is the tensile stress along the length. Magnetostriction λ is modeled as an initial strain acting on the Galfenol

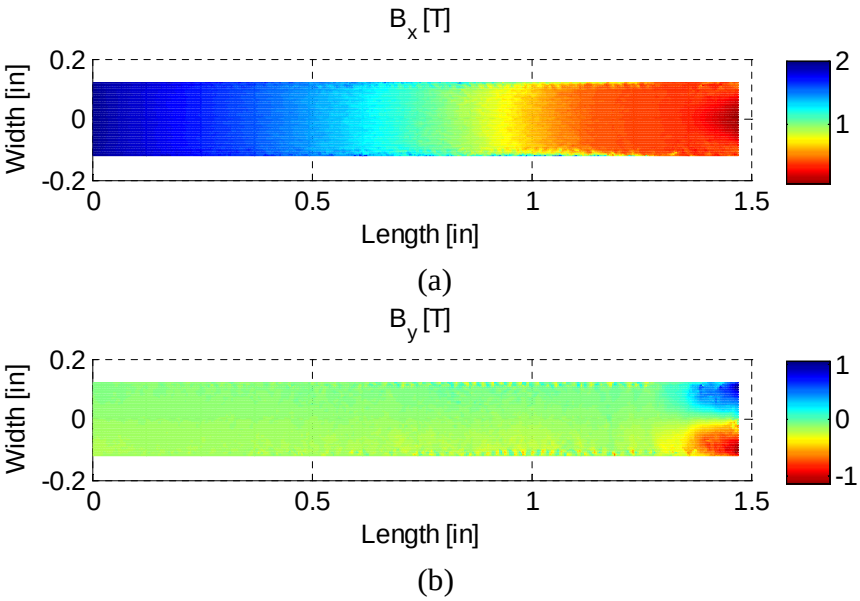

Figure 2. Flux density calculations: (a) B_x: flux density along the length of the Galfenol layer; (b) B_y: flux density along the width.

.

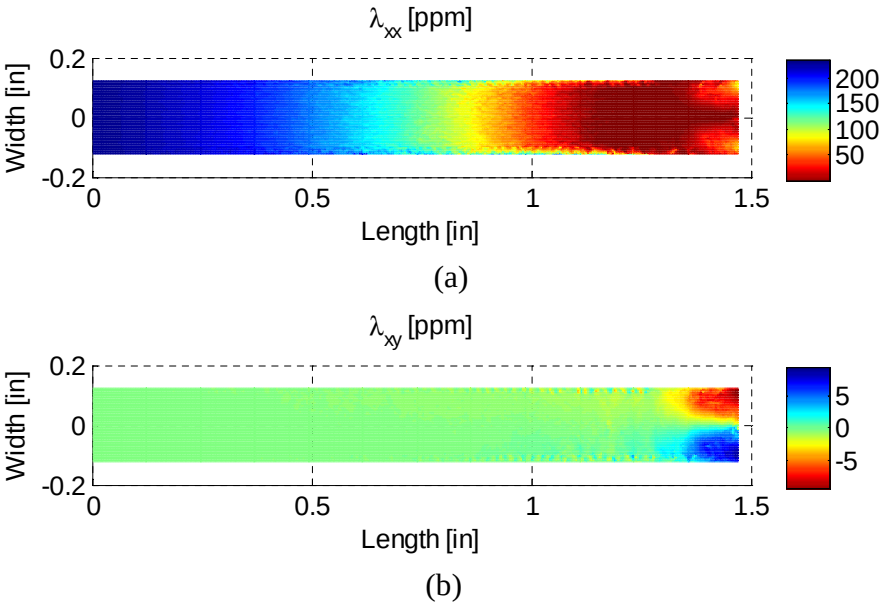

Figure 3. Magnetostriction calculations: (a) λ_{xx}: magnetostriction along the length of the Galfenol layer; (b) λ_{xy}: shear magnetostriction.

domain, starting with the relationship

$$\sigma = E(\epsilon - \epsilon_0), \tag{9}$$

in which σ is the stress tensor, E is the passive Young's modulus of the material, ϵ is the strain tensor and ϵ_0 is the initial strain tensor

$$\epsilon_0 = \begin{bmatrix} \lambda & 0 & 0 \\ 0 & -\lambda/2 & 0 \\ 0 & 0 & -\lambda/2 \end{bmatrix}. \tag{10}$$

To guarantee the volume consistency of the material, the initial strain in the y and z directions induced by λ_{xx} are defined as $-\lambda/2$. Figure 4 shows that $\lambda_{yy}/\lambda_{xx}$ is around -0.5 except near the magnet's end and inside the fixture. In this study, magnetostriction λ is also defined as an interpolation function $\lambda(B_x, T_{xx})$.

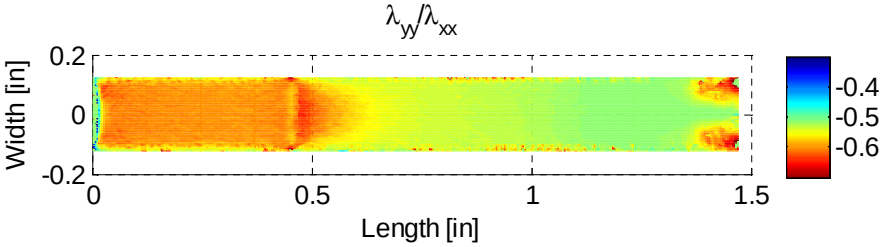

Figure 4. Transverse magnetostriction over longitudinal magnetostriction.

2.3 Rayleigh Damping

The structural damping is modeled as Rayleigh damping such that the damping matrix $\mathbf{C}$ is formed by a linear combination of the mass matrix $\mathbf{M}$ and stiffness matrix $\mathbf{K}$,[23]

$$\mathbf{C} = \alpha\mathbf{M} + \beta\mathbf{K}. \tag{11}$$

Rayleigh damping coefficients α and β can be evaluated from ξ_m and ξ_n, which denote the damping ratio associated with the specific natural frequencies ω_m and ω_n:[24]

$$\begin{bmatrix} \alpha \\ \beta \end{bmatrix} = \frac{2\omega_m\omega_n}{\omega_m^2\omega_n^2} \begin{bmatrix} \omega_n & -\omega_m \\ -1/\omega_n & 1/\omega_m \end{bmatrix} \begin{bmatrix} \xi_m \\ \xi_n \end{bmatrix}. \tag{12}$$

The impulse response of a unimorph beam with a thickness ratio of 2 is shown in Figure 5. The decay curve best fits the measurement for a damping ratio of 0.0076. The natural frequency (244 Hz) can be obtained from the power spectrum of the impulse response. Assuming that the damping ratio is the same for the natural frequency and the second harmonic, α and β can be directly calculated. Table 2 shows the damping ratio, thickness ratio and tip masses of 5 different unimorph beams used in this study. The damping ratio of each unimorph is different because the glue layer varies.

3. EXPERIMENTS

In previous research, Yoo and Flatau[12] placed a Galfenol unimorph harvester directly on the surface of a shaker head. In that configuration, the magnetic field generated by the shaker coil can disturb the Galfenol response. As shown in Figure 6, an aluminum stage is designed in this study to separate the Galfenol beam

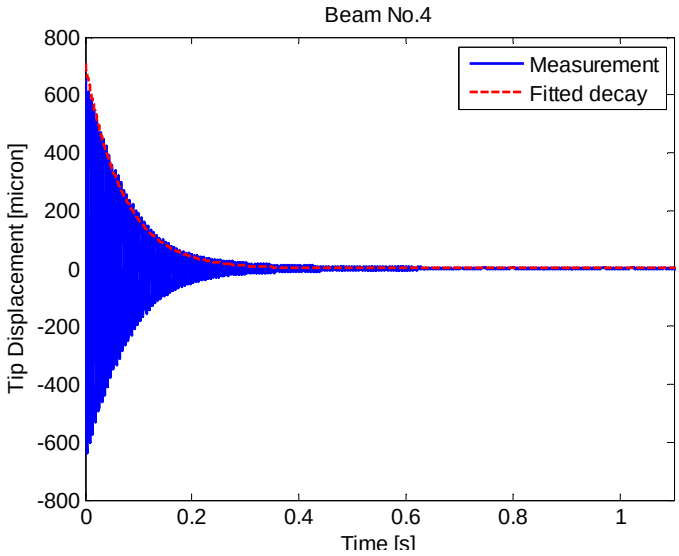

Figure 5. Impulse response of the Galfenol unimorph beam with a thickness ratio of 2.

Table 2. Beam geometries and damping ratios.

Beam No.	1	2	3	4	5
Thickness Ratio	0.3	2/3	1.25	2	3
Damping Ratio	0.0076	0.0078	0.0127	0.006	0.012
Tip Mass (g)	3.22	3.22	3.62	3.78	3.78

from the magnetic field induced by the shaker's drive coil. The unimorph beam sits 11.176 cm (4.4 in.) above the shaker head, where the measured interference from the shaker's coil is negligible. All the components except the unimorph beam and magnets are made of either non-magnetic aluminum or brass to minimizes their influence on the magnetic field. Further details are shown in Figures 6 and 7.

4. MODEL AND PARAMETRIC STUDY

4.1 Model Validation

The 2D FEA model for Galfenol-based unimorph beams is validated using measurements from the 5 unimorph beams listed in Table. 2. The amplitude of the base vibration is fixed to 9.8 m/s^2 throughout the experiments. Experimental measurements and model calculations are compared in Figures 9 and 10. Figure 9 shows that the flux density through the cross-section of the pickup coil is accurately described. However, the voltage calculation is less accurate due to the derivative involved in relation (8). Since the amplitude of the output voltage is determined by the amplitude of the flux density variation, the range of the calculated output voltage is close to the measured data.

In order to simplify the simulations, no moving mesh technique is implemented, thus the voltage induced by the moving tip magnet is not considered. The unimorph with a larger thickness ratio provides a lower amplitude of tip displacement at the resonance frequency, hence the voltage generated by the tip magnet's movement is less significant. Figures 9 and 10 demonstrate that the error of the voltage simulation decreases

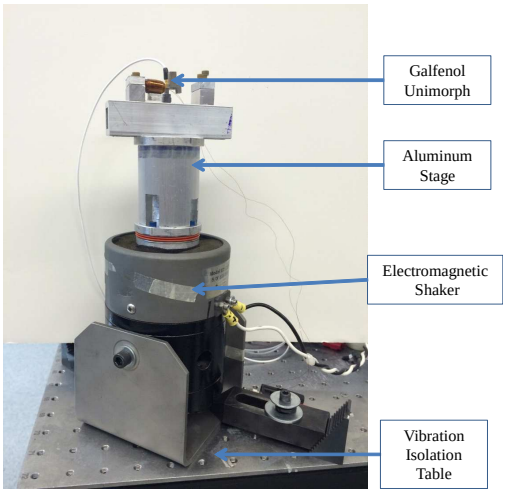

Figure 6. View of the shaker, mounting and isolation stages, and unimorph beam.

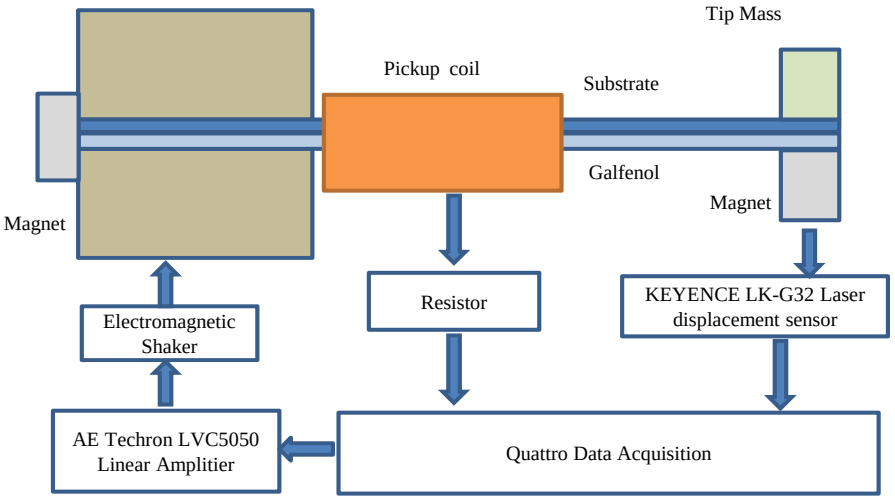

Figure 7. Experiment layout.

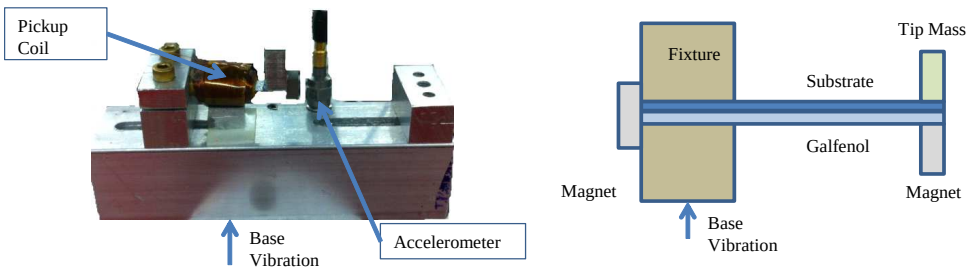

Figure 8. Cantilever Galfenol unimorph harvester.

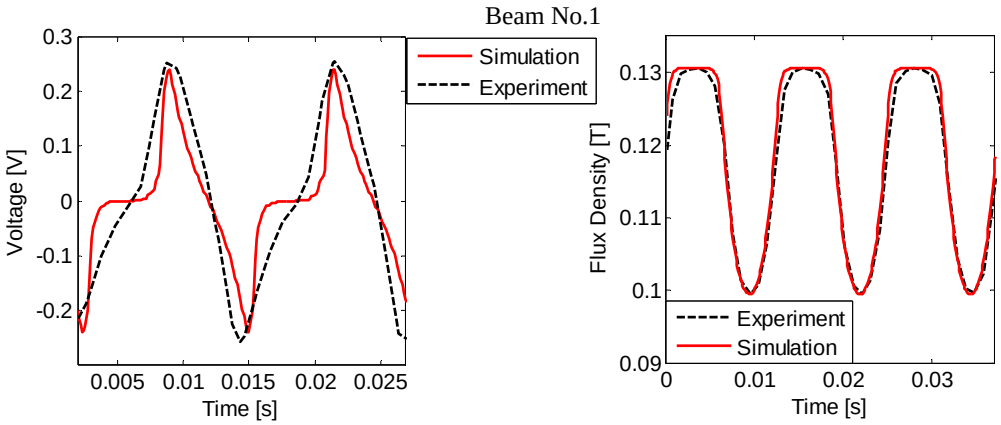

Figure 9. Pickup coil voltage and flux density through the cross-section of the pickup coil for beam No. 1.

as the thickness ratio increases. The accuracy of the calculations may improve in the future with the implementation of a moving mesh technique.

4.2 Pickup coil size

The voltage scavenged from the bending unimorph beam increases monotonically with pickup coil size. However, the outer layers of the coil become insensitive to the flux change through the Galfenol layer as the size of coil increases. On the other hand, the resistance of the coil also increases with coil size and limits the coil's output power. Hence, optimal parameters for the pickup coil should be found.

In this study, the wire gauge size of the pickup coil is 36 (American Wire Gauge) and the length of the pickup coil is fixed to 15.24 mm (0.6 in.). Based on experience, the number of turns per layer is 40 and the thickness per layer is 0.213 mm (0.0084 in.). To guarantee the unimorph beam not touching the coil during bending, the inner layer of the coil is 0.762 mm (0.03 in.) away from the beam surface. Assuming that the electrical load is resistive, the only parameter that needs to be studied is the number of turns of the pickup coil.

In this parametric study, bending of the unimorph beam is neglected and the flux density variation through the Galfenol layer is assumed to follow a 100 Hz, 0.25 T amplitude sinusoidal wave. Figure 11 shows that the output voltage increases with respect to the number of turns. The output voltage reaches saturation when the coil is over 4,000 turns and the maximum output power reaches a peak when the number of turns is around 800.

4.3 Load Match

Different resistive loads are connected to the pickup coil, and the output power is quantified by the average power P_{rms} and the average power density D_{rms},

$$P_{rms} = \frac{\int_0^t (V^2/R)dt}{t}, \quad D_{rms} = P_{rms}/V_{eff}, \tag{13}$$

where V is the voltage measured across the load, R is the resistance of the load, and V_{eff} is the effective volume of the Galfenol layer. In this study, the geometry of the Galfenol layer is 38.1 mm×6.35 mm×0.381 mm

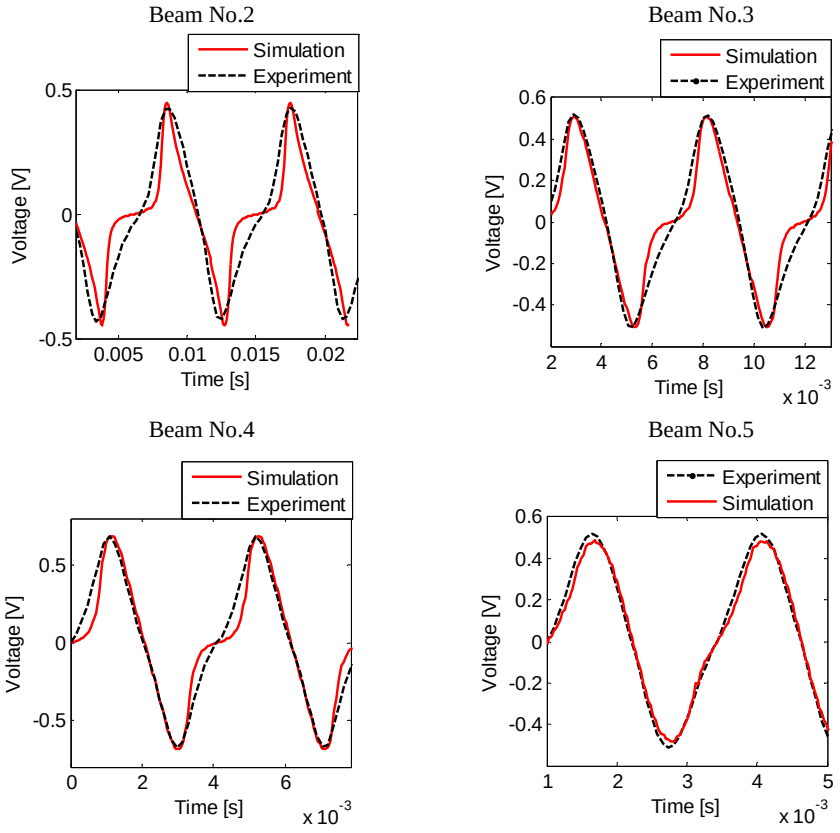

Figure 10. Pickup coil voltage for beams No. 2–5.

(1.5 in.×0.25 in.×0.015 in.), but 11.43 mm (0.45 in.) of the Galfenol layer is clamped inside the fixture and does not generate flux variations. An effective length of 26.67 mm (1.05 in.) is used to calculate the power density. The maximum values of P_{rms} and D_{rms} are observed in beam No. 4, giving 0.90 mW and 13.97 mW/cm^3 respectively.

The pickup coil resistance has a value of 36.8 Ω. According to Figure 12, the maximum value of P_{rms} is achieved when the load resistance R_{load} is slightly larger than the resistance of the pickup coil R_{coil}, because of the inductance of the coil. The following parametric studies ignore the dynamics of the pickup coil. Hence, the maximum power is assumed to occur when $R_{coil} = R_{load}$. The maximum P_{rms} can be estimated from the open-circuit voltage V_{open} and the pickup coil resistance R_{coil},

$$P_{rms} = \frac{\int_0^t (V_{open}^2/4R_{coil})dt}{t}. \tag{14}$$

4.4 Thickness ratio

Type 316 stainless steel with a modulus of around 200 GPa is selected as the substrate material in this study. Epoxy glue Bond-200 (Vishay Intertechnology Inc.) is used to bond the Galfenol layer and the substrate

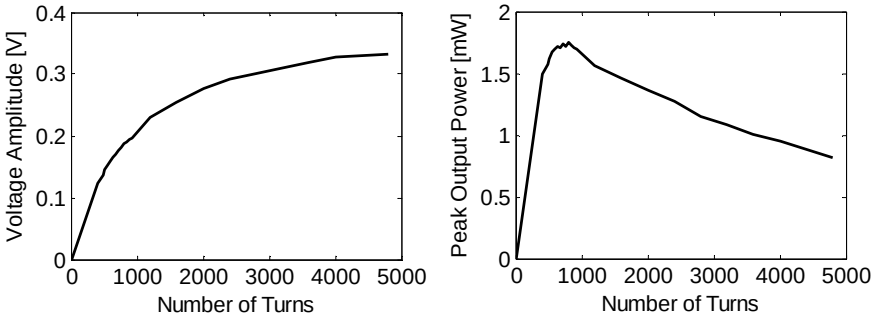

Figure 11. Parametric study results for the pickup coil: Left: open-circuit voltage; Right: output power.

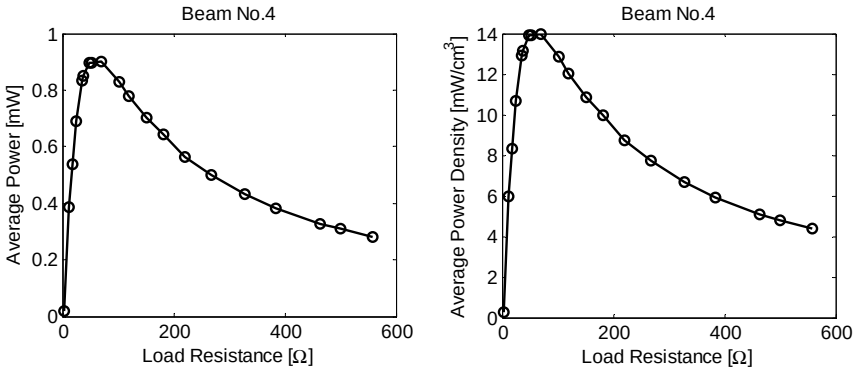

Figure 12. Output power versus load resistance for beam No. 4.

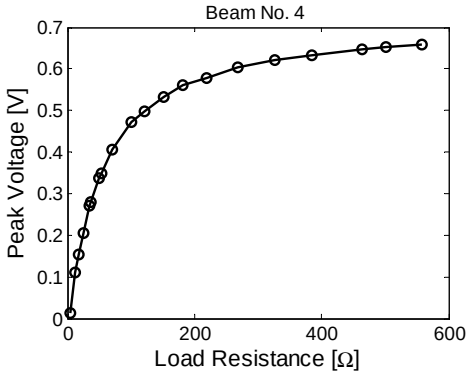

Figure 13. Peak output voltage versus load resistance for beam No. 4.

layer. Based on the assumption of a perfect bonding and the Euler-Bernoulli beam theory, increasing the thickness of the substrate layer helps to push the Galfenol layer away from the neutral plane thus generating more compressive stress in the Galfenol element. However, the tip displacement keeps decreasing as the thickness ratio increases. Hence, an optimal thickness ratio exists.

In this parametric study, the amplitude of the base acceleration is 9.8 m/s^2, the remanent flux density of the tip magnet is 1.8 T, the tip mass is 3.78 gram, the Rayleigh coefficients are $\alpha = 11, \beta = 3.5 \times 10^{-6}$, and the maximum average power is estimated using (14). As shown in Figure 14, the maximum value of V_{open} is observed at a thickness ratio of 1.5 and the maximum value of P_{rms} occurs at a thickness ratio of 2.

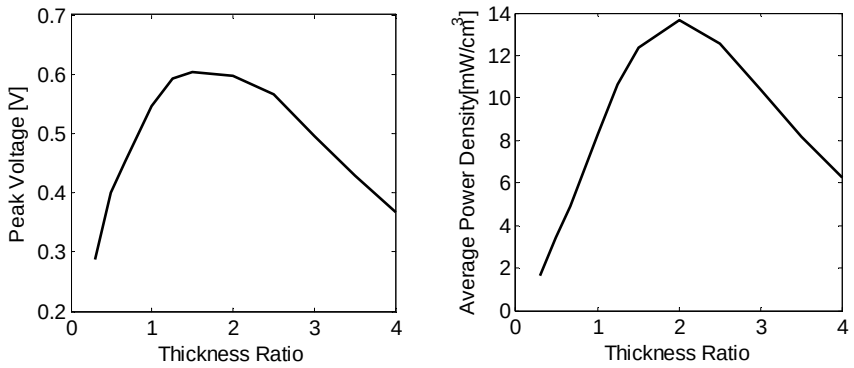

Figure 14. Thickness ratio optimization. Left: Open-circuit voltage amplitude; Right: Average power density.

4.5 Bias magnetic field strength

The tip permanent magnet not only generates a bias magnetic field but also induces voltage in the pickup coil through its own movement. The latter is neglected in this study. The permanent magnet selected in this study applies a pull force of 12.01 N (2.7 lbf) corresponding to 1.8 T remanent flux density. As shown in Figure 8, a magnet is glued on the tip of the cantilever beam while at the fixture end various configurations are studied including no magnets or up to 3 magnets. Figure 15 illustrates that the unimorph harvester generates the highest output voltage without magnets on the fixture end. The optimal remanent flux density of the tip magnet centers the operation of the Galfenol element in the middle of the burst region.

According to the results in previous step, only the unimorph with a thickness ratio of 2 is analyzed in this parametric study. Final simulation results in Figure 16 show that the optimal remanent flux density value of the tip magnet is 1.2 T.

5. SUMMARY AND FUTURE WORK

This paper developed an efficient and accurate 2D FE model for Galfenol unimorph harvesters. A parametric study on the effect of pickup coil size, load resistance, thickness ratio, and bias magnetic field strength on harvester performance were presented. The optimal coil size has 800 turns and the optimal load resistance is around 49.1 Ω for Beam No. 4. Selection of an optimal thickness ratio has to be done considering either

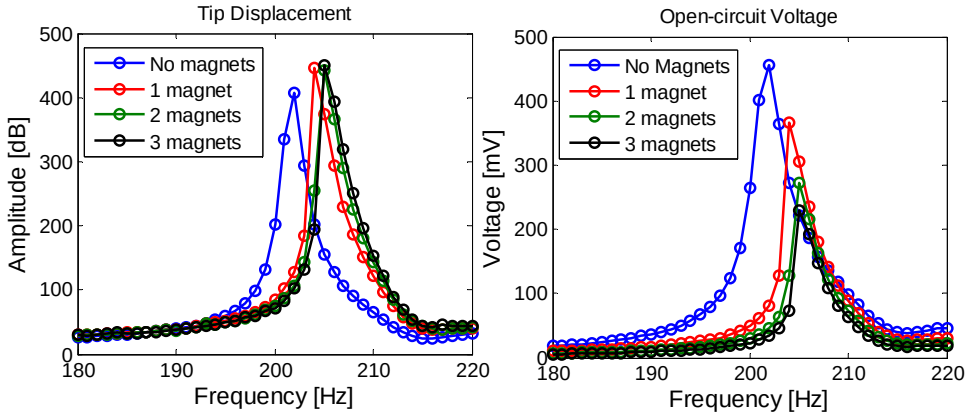

Figure 15. Experiments for various permanent magnet configurations on the fixture side for beam No. 3. Left: tip displacement; Right: open-circuit voltage amplitude.

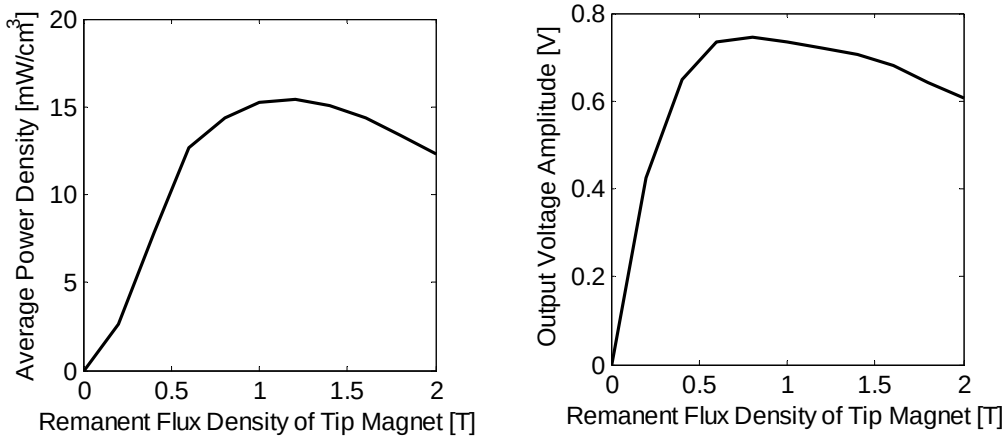

Figure 16. Tip magnet optimization for beam No. 4: Left: average power density; Right: open-circuit voltage amplitude.

voltage output or power density, since both cannot be achieved simultaneously. For this reason, the optimal thickness ratio ranges between 1.5 (maximum voltage) and 2 (maximum power). Further, the calculated power density depends on whether only the active Galfenol section is considered. The optimal remanent flux density of the tip magnet is 1.2 T.

In the future, a parametric study for the tip mass should be designed and different substrate materials need to be compared with stainless steel. A more complete electric circuit has to be designed including resistive and inductive elements to more closely match the impedances. The glue layer and pickup coil dynamics must be considered to improve model accuracy. Ferrari et al.[25] and Erturk et al.[26] implemented strategies to improve the bandwidth of a cantilever piezoelectric harvester, and similar approaches for Galfenol unimorph harvesters will be tested. Current experiments and simulations are limited to sinusoidal base excitations; research on improving the efficiency of harvesting energy from general vibration sources will be conducted followed a study by Daqaq[27] that analyzed a bistable system driven by white and exponentially correlated Gaussian noise.

ACKNOWLEDGMENTS

We wish to acknowledge the member organizations of the Smart Vehicle Concepts Center, a National Science Foundation Industry/University Cooperative Research Center (www.SmartVehicleCenter.org) established under NSF Grant IIP-1238286.

REFERENCES

1. A. E. Clark, M. Wun-Fogle, J. B. Restorff, and T. A. Lograsso, "Magnetostrictive properties of Galfenol alloys under compressive stress," *Materials Transactions*, vol. 43, no. 5, pp. 881–886, 2002.
2. J. Restorff, M. Wun-Fogle, A. Clark, and K. Hathaway, "Induced magnetic anisotropy in stress-annealed Galfenol alloys," *Magnetics, IEEE Transactions on*, vol. 42, no. 10, pp. 3087–3089, 2006.
3. M. Wun-Fogle, J. Restorff, and A. Clark, "Magnetomechanical coupling in stress-annealed Fe–Ga (Galfenol) alloys," *Magnetics, IEEE Transactions on*, vol. 42, no. 10, pp. 3120–3122, 2006.
4. R. Kellogg, A. Flatau, A. Clark, M. Wun-Fogle, and T. Lograsso, "Temperature and stress dependencies of the magnetic and magnetostrictive properties of $Fe_{0.81}Ga_{0.19}$," *Journal of Applied Physics*, vol. 91, no. 10, pp. 7821–7823, 2002.
5. S. Meninger, J. O. Mur-Miranda, R. Amirtharajah, A. Chandrakasan, and J. H. Lang, "Vibration-to-electric energy conversion," *Very Large Scale Integration (VLSI) Systems, IEEE Transactions on*, vol. 9, no. 1, pp. 64–76, 2001.
6. P. Glynne-Jones, M. Tudor, S. Beeby, and N. White, "An electromagnetic, vibration-powered generator for intelligent sensor systems," *Sensors and Actuators A: Physical*, vol. 110, no. 1, pp. 344–349, 2004.
7. S. P. Beeby, M. J. Tudor, and N. White, "Energy harvesting vibration sources for microsystems applications," *Measurement Science and Technology*, vol. 17, no. 12, p. R175, 2006.
8. S. Roundy, P. K. Wright, and J. Rabaey, "A study of low level vibrations as a power source for wireless sensor nodes," *Computer Communications*, vol. 26, no. 11, pp. 1131–1144, 2003.
9. A. Erturk, J. Hoffmann, and D. Inman, "A piezomagnetoelastic structure for broadband vibration energy harvesting," *Applied Physics Letters*, vol. 94, no. 25, pp. 254102–254102, 2009.
10. L. Wang and F. Yuan, "Vibration energy harvesting by magnetostrictive material," *Smart Materials and Structures*, vol. 17, no. 4, p. 045009, 2008.

11. V. Berbyuk, "Vibration energy harvesting using Galfenol-based transducer," in *SPIE Smart Structures and Materials+ Nondestructive Evaluation and Health Monitoring*, pp. 86881F–86881F, International Society for Optics and Photonics, 2013.
12. J. H. Yoo and A. B. Flatau, "A bending-mode Galfenol electric power harvester," *Journal of Intelligent Material Systems and Structures*, vol. 23, no. 6, pp. 647–654, 2012.
13. J.-H. Yoo, A. Flatau, and A. Purekar, "Performance of Galfenol energy harvester at high temperature," in *ASME 2011 Conference on Smart Materials, Adaptive Structures and Intelligent Systems*, pp. 391–396, American Society of Mechanical Engineers, 2011.
14. T. Ueno and S. Yamada, "Performance of energy harvester using iron–gallium alloy in free vibration," *Magnetics, IEEE Transactions on*, vol. 47, no. 10, pp. 2407–2409, 2011.
15. S. Chakrabarti and M. J. Dapino, "Nonlinear finite element model for 3d Galfenol systems," *Smart Materials and Structures*, vol. 20, no. 10, p. 105034, 2011.
16. Z. Deng and M. J. Dapino, "Characterization and finite element modeling of Galfenol minor flux density loops," in *SPIE Smart Structures and Materials+ Nondestructive Evaluation and Health Monitoring*, pp. 86890V–86890V, International Society for Optics and Photonics, 2013.
17. B. Rezaeealam, T. Ueno, and S. Yamada, "Finite element analysis of Galfenol unimorph vibration energy harvester," *Magnetics, IEEE Transactions on*, vol. 48, no. 11, pp. 3977–3980, 2012.
18. W. Armstrong, "An incremental theory of magneto-elastic hysteresis in pseudo-cubic ferromagnetostrictive alloys," *Journal of Magnetism and Magnetic Materials*, vol. 263, no. 1, pp. 208–218, 2003.
19. P. Evans and M. Dapino, "Efficient magnetic hysteresis model for field and stress application in magnetostrictive Galfenol," *Journal of Applied Physics*, vol. 107, no. 6, pp. 063906–063906, 2010.
20. C. Kittel, "Physical theory of ferromagnetic domains," *Reviews of Modern Physics*, vol. 21, no. 4, p. 541, 1949.
21. L. Shu, M. J. Dapino, P. G. Evans, D. Chen, and Q. Lu, "Optimization and dynamic modeling of Galfenol unimorphs," *Journal of Intelligent Material Systems and Structures*, vol. 22, no. 8, pp. 781–793, 2011.
22. L. Shu, L. M. Headings, M. J. Dapino, D. Chen, and Q. Lu, "Nonlinear model for Galfenol cantilevered unimorphs considering full magnetoelastic coupling," *Journal of Intelligent Material Systems and Structures*, vol. 25, no. 2, pp. 187–203, 2014.
23. Z. Kiral, "Damped response of symmetric laminated composite beams to moving load with different boundary conditions," *Journal of Reinforced Plastics and Composites*, vol. 28, no. 20, pp. 2511–2526, 2009.
24. R. W. Clough and J. Penzien, *Dynamics of Structures*, vol. 634. McGraw-Hill New York, 1993.
25. M. Ferrari, V. Ferrari, M. Guizzetti, B. Andò, S. Baglio, and C. Trigona, "Improved energy harvesting from wideband vibrations by nonlinear piezoelectric converters," *Sensors and Actuators A: Physical*, vol. 162, no. 2, pp. 425–431, 2010.
26. A. Erturk and D. Inman, "Broadband piezoelectric power generation on high-energy orbits of the bistable duffing oscillator with electromechanical coupling," *Journal of Sound and Vibration*, vol. 330, no. 10, pp. 2339–2353, 2011.
27. M. F. Daqaq, "Transduction of a bistable inductive generator driven by white and exponentially correlated gaussian noise," *Journal of Sound and Vibration*, vol. 330, no. 11, pp. 2554–2564, 2011.